# Multiple scattering of MeV atomic and molecular ions traversing ultrathin films

D. Zajfman, G. Both,* E. P. Kanter, and Z. Vager†
*Argonne National Laboratory, Argonne, Illinois 60439*
(Received 5 September 1989)

We have investigated the connection between small-angle multiple scattering and charge-changing processes for fast atomic and molecular ions traversing ultrathin solid targets. Results for the atomic ions show a strong target-thickness dependence of the measured final-charge-state distributions. There is also an accompanying dependence of the multiple-scattering widths upon the final charge state of the ions. These results demonstrate conditions far from equilibrium for these processes. A Monte Carlo simulation of particle motion in the foil is described that successfully accounts for these observations. The same simulation is applied to describe the multiple scattering of diatomic molecular ions and to compute the spread of the internuclear velocity after Coulomb explosion. It is found that the Coulomb repulsion tends to reduce multiple-scattering components along the internuclear axis. Consequences for Coulomb-explosion studies of molecular structures are discussed.

## I. INTRODUCTION

Recent studies of the foil-induced dissociation of fast (MeV) molecular ions have demonstrated a novel approach to the problem of determining the geometric structures of molecular ions.[1] In these so-called "Coulomb explosion" experiments,[2] a well-collimated beam of molecular ions strikes a thin target foil. The valence electrons of the molecules are rapidly stripped in this foil, leaving several atomic fragment ions which repel each other due to the mutual Coulomb forces. It has been shown that measurements of the laboratory velocities of all of the resulting fragment ions can be used to determine the internuclear geometry preceding the dissociation for *every* molecule in the beam.[3]

Coulomb explosion experiments, aimed at studying the nuclear vibrations within polyatomic molecular ions,[1] have necessitated the development of ultrathin stripper foils with low multiple-scattering characteristics.[4] A criterion for how thin such strippers should be is to compare the half-width, due to multiple scattering, of the measured velocity distributions to that caused by bond length variations in the molecule due to zero-point vibrations. Ideally, the former should be smaller than the latter. For 4.5-MeV $H_2O^+$ (a typical molecular-ion beam), a low-$Z$ target of $\sim 0.5$ $\mu g/cm^2$ would make those two quantities comparable, assuming multiple scattering and the Coulomb explosion to be independent processes (corrections to this assumption will be described below).

Ultrathin targets offer several other advantages in such experiments. For example, for shorter dwell times in the target, the less important are other solid-state effects in determining the final velocities of the fragment ions. Such effects include the electronic polarization of the solid and the charge-state fluctuations of the dissociation fragments while in the target. For these reasons, ultrathin strippers have recently been employed in these experiments.

## II. PROPERTIES OF ULTRATHIN TARGETS

We have recently described a procedure for preparing ultrathin ($< 1$-$\mu g/cm^2$) films of Formvar.[4] In order to characterize the thickness of these films, we have measured the angular spread of well-collimated monatomic ion beams passing through such targets. While in the target, the ions undergo rapid electron loss and subsequent charge exchange, as well as small-angle nuclear scattering events. The effects of these processes on the ion beam are dependent on the target thickness. For example, for targets thicker than about 1 $\mu g/cm^2$, the charge-state distributions of 3.4-MeV $C^+$ and 4.5-MeV $O^+$ ions are found to be equilibrated (for the most populous charge states near the center of the distribution). Specifically, the fractional yields of these charge states are independent of further target thickness increase and the angular distributions of these ions are found to be independent of the final charge state. A parametrization[5] has been found to yield reliable results under such conditions.[6]

Such theories assume charge-exchange equilibration in the foil and use screened ion-atom potentials characterized by a *constant* mean charge. Therefore the resulting multiple-scattering distributions are independent of the final charge states. Under equilibrium conditions, it is thus possible to estimate the target thickness from a measurement of the angular distributions of the exiting ions.

For foils thinner than about 1 $\mu g/cm^2$, the charge-state distribution is not yet equilibrated, exhibiting a strong dependence upon the target thickness. Furthermore, for such thin targets, the observed angular distributions increase in width with increasing final charge state (see Fig. 1). Such phenomena cannot be explained by multiple-scattering theories, such as Sigmund-Winterborn, but rather must be described as plural scattering. In order to obtain the thicknesses of such very thin films, and to simulate the effects of plural scatterings on the Coulomb explosions of molecular ions, we have developed a Monte

 

Carlo simulation of the passage of fast ions through ultrathin films incorporating both charge-exchange and small-angle scattering. The details of this calculation are described in the Appendix.

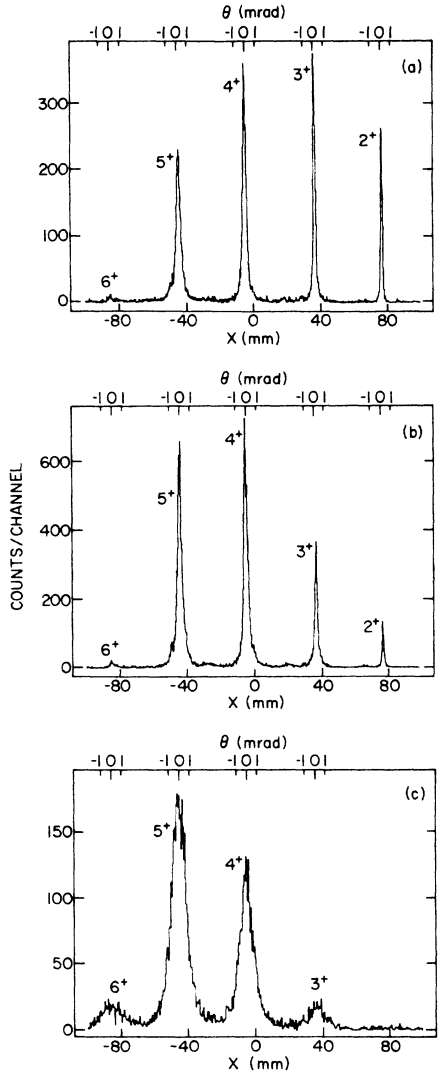


FIG. 1. Charge-state resolved angular scattering distributions of 4.5-MeV $O^+$ penetrating ultrathin Formvar films. (a) and (b) are for films determined to be 0.3 and 0.5 $\mu g/cm^2$, respectively. The charge states of the emerging ions are indicated at the corresponding peaks. The lower abscissas show the positions on the detector surface (in mm), while the upper abscissas give the scattering angles for each charge state (in mrad). The charge states were dispersed by an electrostatic field. Both distributions were measured with targets of preequilibrium thicknesses. For comparison (c) shows the corresponding distribution of 4.5-MeV $O^+$ penetrating a 3.5-$\mu g/cm^2$ carbon foil, which is sufficiently thick to achieve charge-state equilibration.

## III. RESULTS

### A. Monatomic ion beams

As a test of this procedure, we have used it to compute the full width at half-maximum (FWHM) for the angular distributions of nitrogen ions, in various charge states, after passage of 3.7-MeV $N^+$ ions through 1.6- and 4.6-$\mu g/cm^2$ carbon targets. At this velocity, such target thicknesses are sufficient to achieve charge-state equilibrium. Thus, for final charge states $q$ in the range $1 \leq q \leq 5$, these angular widths are independent of $q$.[6] This is not true for the rare charge states $q=6$ and 7, which require much longer equilibration lengths.[6,7] We thus restrict our simulation to consider only charge-changing in the $L$ shell. As is shown in Fig. 2, the results of the simulation agree very well with the experimental data. As expected, for $q<6$ there is no significant charge-state dependence to the angular widths in either the simulation or experiment.

For comparison under nonequilibrium conditions, we have computed the FWHM for the angular distributions of oxygen ions emerging from Formvar targets and adjust the target thickness used in the simulations to get the best fit to the experimental charge-state distributions. With the thicknesses thus constrained, we compare the resultant angular distributions of oxygen ion in different charge states to experiment. The results, shown in Figs. 3 and 4, are found to be consistent with the data. In this nonequilibrium region, the angular FWHM's display a strong dependence on the final charge state. This can be understood by the fact that under these conditions, because of the dominance of single-electron loss, a larger number of collisions (and with smaller impact parame-

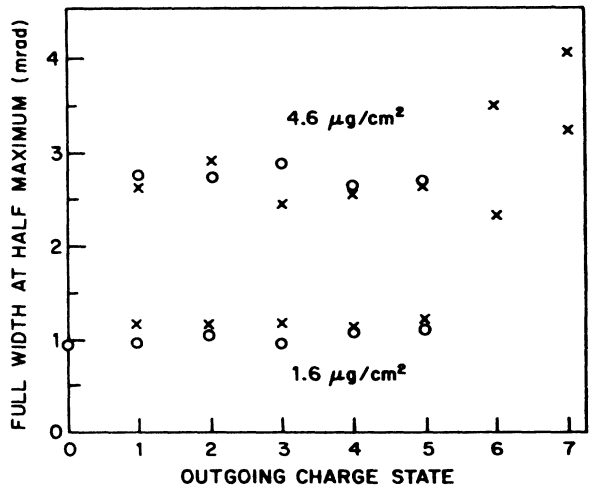


FIG. 2. Full width at half-maximum (FWHM) of the angular distributions of nitrogen ions emerging in various charge states from 1.6- and 4.6-$\mu g/cm^2$ carbon targets following impact of 3.7-MeV $N^+$ ions. Crosses are the FWHM of best-fit Gaussian profiles to the data. Circles result from similar analysis of the angular distributions derived from each charge state from the Monte Carlo simulations described in the text.

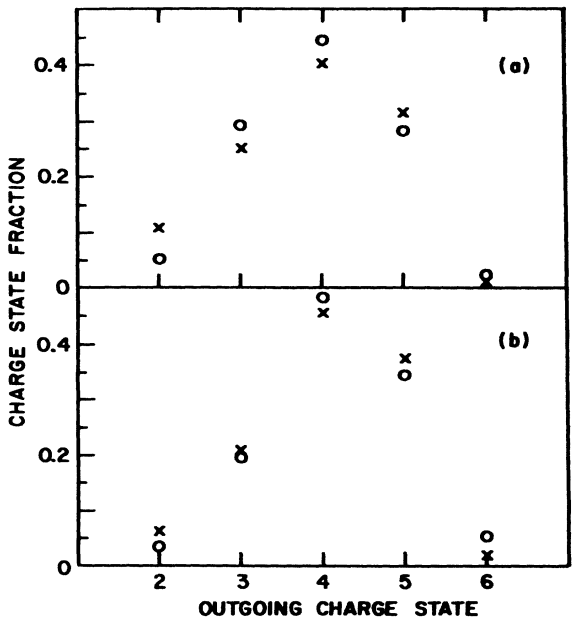


FIG. 3. Preequilibrium charge-state distributions of oxygen ions emerging from ultrathin Formvar films following impact of 4.5-MeV $O^+$ ions. (a) 0.3-$\mu g/cm^2$ Formvar target, (b) 0.5-$\mu g/cm^2$ Formvar target. Crosses are the experimental data, while circles show the results of the Monte Carlo simulation after varying the target thickness to fit the experimental data.

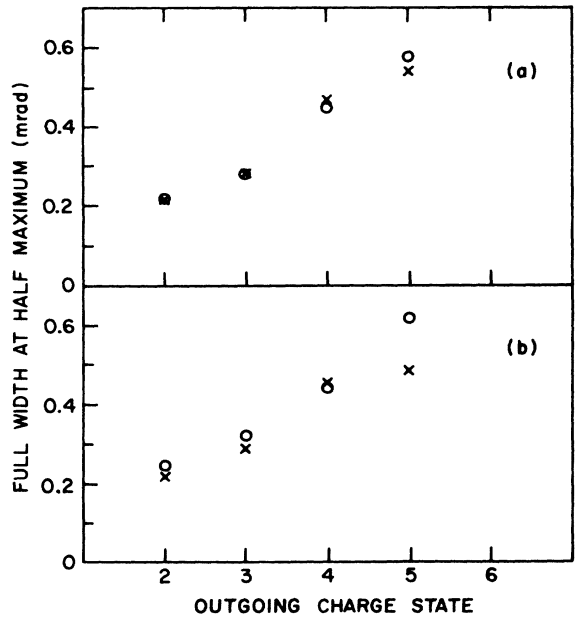


FIG. 4. FWHM of angular distributions of oxygen ions emerging from ultrathin Formvar films, as a function of the oxygen final charge state, following impact of 4.5-MeV $O^+$. (a) and (b) and symbols as in Fig. 3.

ters) are required to produce the higher charge states. This correlation is reproduced in the simulation, demonstrating that such targets approach single-collision conditions. This effect is absent in the equilibrium data (and simulation) where the competition between capture and loss is sufficient for memory of the charge-state history to be "lost."

### B. Molecular ion beams

In the case of molecular projectiles traversing thin films, in addition to multiple scattering, the trajectories are modified by the mutual Coulomb repulsion of the ionic fragments. A simplified treatment of this effect is to assume these are independent interactions producing additive small-angle deflections.[8] A statistical treatment using the Fokker-Planck equation to simultaneously incorporate these two effects demonstrated[9] that focusing and defocusing effects are not accounted for in the simpler model. The Gaussian approximation of the Fokker-Planck approach neglects the important tails of realistic multiple-scattering distributions.[10] We have addressed this deficiency by incorporating the Coulomb explosion of a diatomic molecule within the framework of the Monte Carlo calculation described above.

For a molecule with its internuclear axis aligned to the beam direction, the multiple-scattering deflections are perpendicular to the Coulomb explosion forces, and we expect the multiple scattering to be independent of the dissociation process for these molecules (the energy straggling effects are generally much smaller than angular scattering and are ignored here). We therefore restrict our discussion to molecules aligned transverse to the beam direction in order to explore the interplay between Coulomb explosion and multiple scattering.

The method of computation is nearly identical to the monatomic case except that now the projectile consists of two independent atoms, traveling at the same velocity through the target, undergoing multiple scattering, and interacting with each other via their Coulomb fields. In the center of mass of the molecule, the motion of the particles is essentially planar (i.e., in the plane perpendicular to the beam axis). Thus, at each step, the distance of travel, the scattering angle, and the charge state are first computed independently for each fragment ion and then their coordinates and velocities are corrected for the Coulomb repulsion. The result of this procedure produces the final positions and velocities $\mathbf{V}_1$ and $\mathbf{V}_2$ for both ions at the exit of the target foil. The magnitude of the asymptotic relative velocity $\mathbf{V}$ is determined by energy conservation by

$$V=\left[U^2+\frac{2Q_1Q_2}{\mu r}\right]^{1/2}, \tag{1}$$

where $Q_1$ and $Q_2$ are the final charge states of the fragment ions, $\mu$ is the reduced mass of the molecule, and $r$ is the internuclear distance between the fragments at the exit of the foil. The relative velocity between the fragments at the same point is

$$\mathbf{U}=\mathbf{U}_1-\mathbf{U}_2 . \tag{2}$$

We choose the convention that $\mathbf{r}$ initially lies on the $x$ axis. To compute the asymptotic angle of rotation of the internuclear axis we use the fact that, in the post-foil region where the fragments interact only via their Coulomb repulsion, the Runge-Lenz vector defined by

$$R_x=\mu r U_y^2+Q_1Q_2\ ,$$
$$R_y=-\mu r U_y U_x\ , \tag{3}$$
$$R=(R_x^2+R_y^2)^{1/2}$$

is conserved.[11] Then, the final angle of rotation is simply

$$\phi=\mathrm{sgn}(U_y)\arccos\left[\frac{Q_1Q_2}{R}\right]+\arcsin\left[\frac{R_y}{R}\right]\ . \tag{4}$$

We have computed the asymptotic coordinates and charge states for the Coulomb explosion of 4.8-MeV $OH^+$ molecules after dissociation in a thin carbon foil. The result of a typical (4000 molecules) simulation is shown in Fig. 5 in the form of a density plot. The series of elongated patterns show the transverse velocity distributions of the protons which have been influenced by partner oxygen fragments [located at (0,0) in this coordinate system] in differing charge states. The initial orientation of the $OH^+$ molecules was assume to be parallel to the $x$ axis. Figure 6 shows the spread of the angular rotation of the internuclear axis in the $x$-$y$ plane ($\phi$) as a function of the final charge state of the oxygen fragment ion, for different target thicknesses.

It is evident from these figures that the Coulomb force acts as an astigmatic lens on the multiple-scattering broadening in the foil. A spatially uniform force cannot produce such lensing. However, the nonvanishing gradient of the Coulomb force can introduce focusing and defocusing.[9] The geometrical mean of the radial ($\Delta u_r$) and angular ($\Delta u_\phi$) widths is very close to the multiple-scattering width observed for monoatomic oxygen ions. The directional dependence on the gradient in the transverse plane and the preservation of the geometric mean permits these results to be extended to other orientations of the molecule.

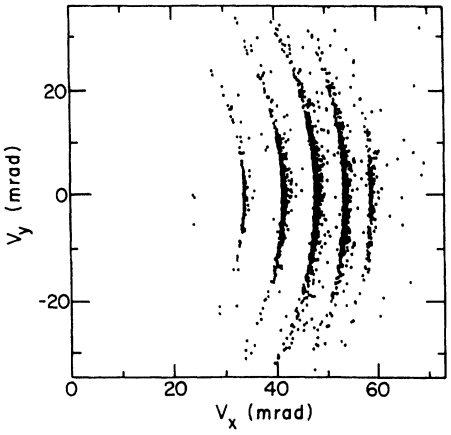


FIG. 5. Density plot of the projection on the $V_x$-$V_y$ plane, as described in text, of the images of fragment ions resulting from the simulated Coulomb explosions of 4000 4.5-MeV $OH^+$ ions dissociated in a 0.5-$\mu$g/cm$^2$ carbon target.

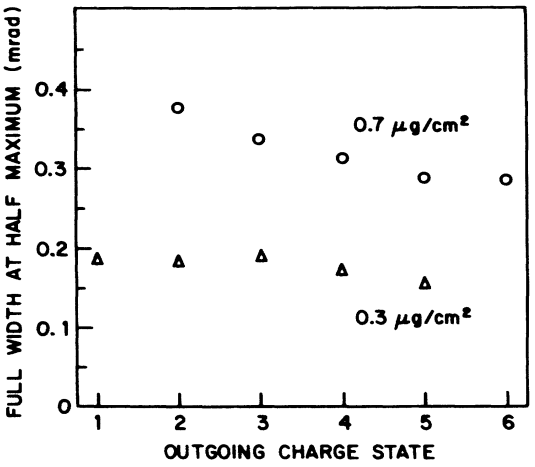


FIG. 6. FWHM of angular distributions for the internuclear axis of the dissociated $OH^+$ molecule, for various final charge states of oxygen fragment ions, emerging 0.3- and 0.7-$\mu$g/cm$^2$ carbon targets. These results were for simulations carried out for impact of 4.8-MeV $OH^+$ ions.

The small radial extent of these distributions implies that the determination of bond lengths of diatomic molecules from Coulomb explosions can be quite precise. To estimate this precision, consider the zero-point vibrations of a very stiff harmonic oscillator, with $\hbar\omega=1$ eV. Then, the spatial density in the ground state is proportional to $\exp[-(x/\sigma)^2]$, where $\sigma^2=\hbar/M_p\omega\simeq 0.004$ Å$^2$ and $M_p$ is the proton mass. Thus the equivalent spread (FWHM) in the radial velocity corresponds to $\sim 2$ mrad, while the simulation shows about 1 mrad for the case of 0.3 $\mu$g/cm$^2$ (see Fig. 2). Clearly, for more realistic vibrations ($\hbar\omega\sim 0.1$ eV or less) the smearing effects of multiple scattering on diatomic bond-length distributions are expected to be even smaller compared to zero-point fluctuations.

From the simulations, we can also estimate the extent to which multiple scattering affects Coulomb explosion measurements of bending vibrations in polyatomic molecules. The spread in $\phi$ (Fig. 6) of 0.2 rad (FWHM) can be described by the zero-point fluctuations in angle of an oscillator with $\hbar\omega=0.25$ eV. This corresponds to a fairly rigid bending motion. Furthermore, this underestimates the limitation on the highest bending frequency because of the neglect of Coulomb gradients in the bending degree of freedom. Thus, from these results, it is apparent that with the ultrathin targets used here Coulomb explosion determinations of molecular structure are not hindered by multiple scattering.

Another point of interest is the $\phi$ dependence on the final charge seen in Fig. 6. The general trends are that the FWHM of the distribution in $\phi$ increases with increasing target thickness. Furthermore, with increasing final charge state, this width decreases. This is the oppo-

site of the trend observed in the angular spread simulations (and experiments) with monatomic ion beams. A part of the explanation for this behavior might be the following. The higher the oxygen charge state, the stronger the post-foil Coulomb repulsion. This repulsion more rapidly increases the moment of inertia of the system thereby limiting the overall amount of rotation of the molecular cluster, thus leading to smaller values of $\phi$ with increasing charge state. The width decrease is not very dramatic because the multiple scattering of the proton dominates over that of the more energetic oxygen fragment, and thus is independent of the oxygen charge state.

## IV. CONCLUSION

The results of these experiments, and corresponding simulations, demonstrate that with ultrathin stripper foils, producing nonequilibrium charge-state distributions, there is a corresponding strong dependence of the angular multiple-scattering widths on the final charge state of the projectile. It is important to recognize the presence of such effects in any experimental tests of heavy-ion multiple-scattering theories. Furthermore, this phenomenon should be considered in the choice of stripping foils in the design of heavy-ion accelerators.

The simulation procedure described here has been used successfully to deduce the thicknesses of ultrathin films of Formvar by simultaneously fitting the nonequilibrium charge-state distributions and $q$-dependent multiple scattering of MeV heavy-ion beams in these films. The simulations of molecular-ion penetration has demonstrated that for most Coulomb-explosion experiments utilizing such thin films as strippers the effects of multiple scattering are negligible, compared to molecular vibrations.

## ACKNOWLEDGMENTS

One of the authors (D.Z.) would like to thank the Argonne Physics Division for their hospitality and for the opportunity to participate in this research. This work was supported by the U.S. Department of Energy, Office of Basic Energy Sciences, under Contract No. W-31-109-ENG-38.

## APPENDIX

### 1. Scattering cross section

The simulations were carried out using the binary collision model described by Moller, Pospiech, and Schrieder.[12] Reduced units for path length $D$ and energy $E$ have been used[13] and are defined by

$$\xi=\frac{4\pi a^2\mu n}{M_1+M_2}D \ , \tag{A1}$$

$$\varepsilon=\frac{aM_2}{Z_1Z_2(M_1+M_2)}E \ . \tag{A2}$$

The subscripts 1 and 2 are for projectile and target, respectively. $M_i$ are the masses, $Z_i$ the atomic numbers, $\mu$ is the reduced mass, $n$ the number of target atoms per unit volume; $a=0.8853(Z_1^{2/3}+Z_2^{2/3})^{-1/2}$ is the screening distance.[13] Atomic units are used throughout.

The reduced scattering cross section is defined as

$$J=\frac{\sigma}{\pi a^2} \ . \tag{A3}$$

The ion-atom potential is assumed to be of the form

$$V(r)=\frac{Z_1Z_2}{r}\phi(r/a) \ , \tag{A4}$$

where $r$ is the projectile target distance and $\phi(r/a)$ is the Thomas-Fermi function.[14] In order to determine the scattering angle at each collision, we need the differential cross section. Lindhard, Nielsen, and Scharff[13] have shown that the differential cross section for such a scattering potential is of the form

$$\frac{dJ}{dz}=\frac{f(z)}{z^2} \ , \tag{A5}$$

where

$$z=\varepsilon\sin\tfrac{1}{2}\alpha \ . \tag{A6}$$

$z$ may be regarded as the reduced quantity for the center-of-mass scattering angle $\alpha$. The function $f(z)$ has been given by Meyer.[15]

We assume that each scattering center will be effective within a spherical volume of radius $r_0$, equal to half the distance of immediately neighboring atoms

$$r_0=\tfrac{1}{2}n^{-1/3} \ . \tag{A7}$$

Thus the reduced total cross section is given by

$$J_{\rm tot}=\left[\frac{r_0}{a}\right]^2 \ . \tag{A8}$$

This restriction results in a minimum scattering angle $z_{\rm min}$, which is determined by the reduced total scattering cross section

$$J_{\rm tot}=\int_{z_{\rm min}}^{\varepsilon}\frac{dJ}{dz'}dz'=J(\varepsilon)-J(z_{\rm min}) \ . \tag{A9}$$

### 2. Mean free path

The distance of travel between successive collisions is determined by a Monte Carlo method. From the definition of the cross section, assuming a random distribution of atoms in the solid, the collision probability $k_a$ is given as a function of the distance of travel $d$ by

$$k_a=1-\exp(-n\sigma_{\rm tot}d) \tag{A10}$$

or, in term of reduced quantities,

$$k_a=1-\exp[-(M_1+M_2)J_{\rm tot}\delta/4\mu] \ , \tag{A11}$$

where $\delta$ is the reduced traveling distance between two successive collisions. Thus, for a given random value of $k_a$ [$k_a$ being uniformly distributed is the interval (0,1)] $\delta$ can be evaluated,

$$\delta=-\frac{4\mu}{M_1+M_2}\frac{\ln(1-k_a)}{J_{\rm tot}} . \tag{A12}$$

### 3. Scattering angle

The reduced scattering angle in the center of mass system at each collision ($z$) can be calculated for a given random number $k_b$ from Eq. (A9)

$$\begin{aligned} k_b&=[J(z)-J(z_{\rm min})]/J_{\rm tot}\\ &=[J(z)-J(\varepsilon)+J_{\rm tot}]/J_{\rm tot} ,\\ z&=J^{-1}[J(\varepsilon)+(k_b-1)J_{\rm tot}] , \end{aligned} \tag{A13}$$

where $J^{-1}$ is the inverse function of $J$. The function $J(z)$ is first integrated [Eqs. (A5) and (A6)] and tabulated in order to reduce computing time, and thus $J(\varepsilon)$ and $z$ can be extracted by interpolation.

The direction of the particle motion is defined by two directional angles $\Theta_i$ (polar) and $\Phi_i$ (azimuthal). At each collision, the azimuthal scattering angle $\psi$ around the axis given by $(\Theta_i,\Phi_i)$ has an isotropic distribution, and can be calculated by

$$\psi=2\pi k_c , \tag{A14}$$

where $k_c$ is another random number ($0\le k_c\le 1$). The current polar scattering angle in the laboratory frame is derived by transforming $z$ [Eq. (A6)] from the center-of-mass system

$$\cos\theta=\left[1-\frac{2\mu z^2}{M_1\varepsilon^2}\right]\left[1-\frac{4\mu z^2}{(M_1+M_2)\varepsilon^2}\right]^{-1/2} . \tag{A15}$$

After each collision, the previous $(\Theta_i,\Phi_i)$ directional angles are connected into new angles $(\Theta_{i+1},\Phi_{i+1})$. For a scattering through $(\theta,\psi)$, we get

$$\begin{aligned} \cos\Theta_{i+1}&=-\sin\theta\cos\psi\sin\Theta_i+\cos\theta\cos\Theta_i ,\\ \cos\phi_{i+1}&=\frac{1}{\sin\Theta_{i+1}}(\sin\theta\cos\psi\cos\Theta_i\cos\Phi_i\\ &\quad-\sin\theta\sin\psi\sin\Phi_i\\ &\quad+\cos\theta\sin\Theta_i\cos\Phi_i) . \end{aligned} \tag{A16}$$

### 4. Loss and capture cross section

In order to determine the charge-state dependence of multiple scattering, we extract the ratio of electron-capture and -loss cross sections from the equilibrium relation

$$F(q)\sigma_l(q,q+1)=F(q+1)\sigma_c(q+1,q) , \tag{A17}$$

where $F(q)$ is the equilibrium charge-state fraction,[16] and $\sigma_l$ and $\sigma_c$ are the loss and capture cross sections, respectively. This relation holds only if multiple-electron processes can be neglected. Studies of ion-atom collision in this velocity range support such an assumption, as multiple charge-changing cross sections are found to be at least an order of magnitude smaller than those for the corresponding single-electron processes.

In order to fix the magnitudes of these cross sections, two additional constraints are imposed.

(i) The electron loss cross section $\sigma_l$ is assumed to be proportional to the current number of $L$-shell electrons in the projectile

$$\sigma_l(q,q+1)=(Z_1-2-q)\sigma_0 , \tag{A18}$$

where $q$ is the current charge state of the projectile (before the collision) and $\sigma_0$ is taken to be the geometrical cross section for the $L$ shell

$$\sigma_0=\pi r_L^2=\left[\frac{n_L^2}{Z_1-2}\right]^2 , \tag{A19}$$

where $r_L$ is the radius of the projectile $L$ shell and $n_L=2$ is the principal quantum number. From this we can extract a critical radius $r_c$ by equating the cross section for electron loss to the area $\pi r_c^2$. We thus find

$$r_c(q)=\frac{n_L^2}{Z_1-2}(Z_1-2-q)^{1/2} . \tag{A20}$$

We assume that whenever the distance of closest approach (see the following section) between the projectile and a target atom is smaller than $r_c$, one electron will be lost from the projectile.

(ii) The capture cross section is given immediately from Eq. (A18)

$$\sigma_c(q+1,q)=\frac{F(q)}{F(q+1)}\sigma_l(q,q+1) . \tag{A21}$$

We can define now a mean free path for capture

$$\lambda_c=\frac{1}{\sigma_c(q+1,q)n_e} , \tag{A22}$$

or in reduced units

$$\delta_c=\frac{4\pi a^2\mu n_e}{M_1+M_2}\lambda_c , \tag{A23}$$

where $n_e$ is the average density of electrons in the target, thus the probability of capture within a given traveling distance between each collision is

$$C=1-\exp(-\delta/\delta_c) . \tag{A24}$$

At each step, we compare this number with a random number $k_d$ chosen so that $0\le k_d\le 1$. When $k_d<C$, capture of one electron is assumed to have occurred during the path between the collision.

### 5. Distance of closest approach

In order to decide if an electron is lost in any given collision (see the previous section), the distance of closest approach has to be calculated. Since the scattering angle $\theta$ is known [Eq. (A15)], the impact parameter $b$ can be evaluated using the Lindhard "Magic Formula"[13]

$$\theta=\left[\frac{-3}{4E^2}b^{1/3}\frac{d}{db}[V^2(b)b^{2/3}]\right]^{1/2} \tag{A25}$$

This gives results of sufficient accuracy in the domain of small scattering angles considered here. To reduce the computing time, the function $\theta(b)$ was computed by table look-up and interpolation for each value of $b$.

The distance of closest approach $r_{\min}$ is related to the impact parameter $b$ by the potential function so that

$$V(r_{\min})=E_{\text{c.m.}}\left[1-\frac{b^2}{r_{\min}^2}\right], \tag{A26}$$

where $E_{\text{c.m.}}$ is the center-of-mass energy.

Using this Monte Carlo formalism, the cumulative effect of multiple small-angle scattering with simultaneous charge-changing collisions is followed for each projectile trajectory. The calculation of each trajectory is terminated when the depth coordinate is equal to the foil thickness.

---

*Present address: Harvard University, Cambridge, MA 02138.
†Also at: Weizmann Institute of Science, Rehovot 76100, Israel.

[1]Z. Vager, R. Naaman, and E. P. Kanter, Science **244**, 426 (1989).
[2]D. S. Gemmell, Chem. Rev. **80**, 301 (1980), and references therein.
[3]I. Plesser, Z. Vager, and R. Naaman, Phys. Rev. Lett. **56**, 1559 (1986); E. P. Kanter, Z. Vager, G. Both, and D. Zajfman, J. Chem. Phys. **85**, 7487 (1986); Z. Vager, E. P. Kanter, G. Both, P. J. Cooney, A. Faibis, W. Koenig, B. J. Zabransky, and D. Zajfman, Phys. Rev. Lett. **57**, 2793 (1986).
[4]G. Both, E. P. Kanter, Z. Vager, B. J. Zabransky, and D. Zajfman, Rev. Sci. Instrum. **58**, 424 (1987).
[5]D. Burch and K. Green, University of Washington, Nuclear Physics Laboratory Annual Report, 1975 (unpublished), p. 186.
[6]E. P. Kanter, Phys. Rev. A **28**, 1401 (1983).
[7]K. Ozawa, H. Yamaguchi, K. Kawatsura, M. Sataka, T. Kitahara, A. Kikuchi, K. Komaki, A. Ootuka, and F. Fujimoto, Nucl. Instrum. Methods B **9**, 621 (1985).
[8]Z. Vager and D. S. Gemmell, Phys. Rev. Lett. **37**, 1352 (1976).
[9]I. Plesser, Nucl. Instrum. Methods **194**, 269 (1982); Z. Vager, Ann. Israel Phys. Soc. **4**, 139 (1981).
[10]P. Sigmund and K. B. Winterbon, Nucl. Instrum. Methods **119**, 541 (1974).
[11]See, e.g., *Group Theory and the Coulomb Problem,* edited by M. J. Englefield (Wiley, New York, 1972), p. 52.
[12]W. Moller, G. Pospiech, and G. Schrieder, Nucl. Instrum. Methods **130**, 265 (1975).
[13]J. Lindhard, V. Nielsen, and M. Scharff, Mat.-Fys. Medd. K. Dan. Vidensk. Selsk. **36**, 10 (1968).
[14]P. Gombas, in *Atome II,* Vol. 36 of *Handbuch der Physik,* edited by S. Flügge (Springer Verlag, Berlin, 1956), p. 109.
[15]L. Meyer, Phys. Status Solidi B **44**, 253 (1971).
[16]A. B. Wittkower and H. D. Betz, At. Data **5**, 113 (1973).